Sparse-sampling methods for hyperspectral infrared microscopy

Geiger, Andreas, Ulcickas, James R., Liu, Youlin, Witinski, Mark, Blanchard, Romain, et al.

Andreas C. Geiger, James R. W. Ulcickas, Youlin Liu, Mark F. Witinski, Romain Blanchard, Garth J. Simpson, "Sparse-sampling methods for hyperspectral infrared microscopy ," Proc. SPIE 10980, Image Sensing Technologies: Materials, Devices, Systems, and Applications VI, 1098016 (13 May 2019); doi: 10.1117/12.2518471

SPIE.

Event: SPIE Defense + Commercial Sensing, 2019, Baltimore, Maryland, United States

Sparse-sampling methods for hyperspectral infrared microscopy

Andreas C. Geiger[a], James R.W. Ulcickas[a], Youlin Liu[a], Mark F. Witinski[b], Romain Blanchard[b], Garth J. Simpson*[a].

[a]Department of Chemistry, Purdue University, West Lafayette, Indiana, 47907, USA
[b]Pendar Technologies LLC., Cambridge, MA, 02138, USA

ABSTRACT

A hyperspectral beam-scanning microscope operating in the long wave infrared (LWIR) is demonstrated for future application to stand-off imaging platforms. A 32-channel quantum-cascade laser (QCL) array enables rapid wavelength modulation for fast hyperspectral imaging through sparse sampling in position and wavelength, which when coupled with image reconstruction techniques can enhance frame rate. Initial measurements of dichloromethane and water mixtures are shown, utilizing spectral information for classification across the field of view. Ongoing efforts aim to utilize co-propagating visible and IR beams to enhance spatial resolution for the IR measurements by combining spatial information retrieved from visible images obtained concurrently. Future work will leverage Lissajous trajectories for sparsely-sampled beam-scanning and extend the image interpolation algorithms to arbitrary dimension for sparse sampling in the spectral domain. Simulations of the error associated with various sparse-sampling methods are also presented herein which support the use of Lissajous trajectories as a sparse-sampling method in beam-scanning microscopy.

Keywords: quantum cascade laser, hyperspectral imaging, sparse sampling, microscopy

1. INTRODUCTION

Recent threats and attacks in mass-transit settings and at large public events have punctuated the need for development of technologies that can rapidly screen for threats at a safe distance.[1] Ideally, such technologies would be capable of non-invasive and rapid detection of threat compounds such as explosives.[2] These technologies could be employed to screen vehicles in a parking lot or people before they enter a building or public event.[3] IR detection of threat compounds has the advantage of being a non-invasive, eye-safe, and sensitive stand-off technique.[4] Current technologies are capable of rapid spectroscopy or relatively slow hyperspectral imaging for selective threat detection based on the spectral "fingerprint" of

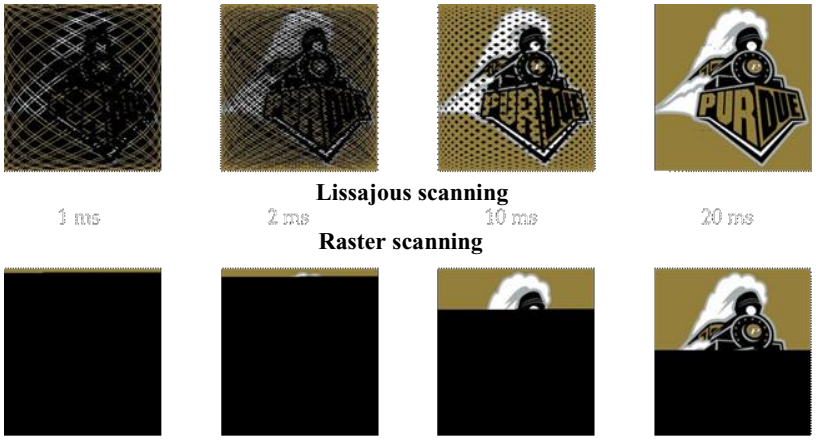

Figure 1. Comparison between beam-scanning sampling trajectories. Lissajous scanning sparsely samples the entire field of view more efficiently than conventional raster scanning.

* gsimpson@purdue.edu

Image Sensing Technologies: Materials, Devices, Systems, and Applications VI, edited by Nibir K. Dhar, Achyut K. Dutta, Sachidananda R. Babu, Proc. of SPIE Vol. 10980, 1098016 · © 2019 SPIE
CCC code: 0277-786X/19/$18 · doi: 10.1117/12.2518471

the threat compound.[5-10] However, conventional spectroscopy is not particularly useful in this application space since a threat compound is typically concentrated in a particular spatial location. Imaging provides information about the spatial location of the threat and improves the signal-to-noise of the measurement since a conventional spectroscopy approach may drown out the spatially localized signal through signal averaging. Yet, current imaging approaches are too slow for application in threat detection. A recently developed beam-scanning hyperspectral stand-off imaging system requires ~19 seconds for image acquisition.[11] It is not realistic to expect that all threats could be detected with such a frame rate. In this work, a hyperspectral microscope operating in the LWIR is demonstrated for future application to stand-off imaging platforms. It is our aim to integrate sparse-sampling methods, into our imaging system to improve the accessible frame rate. We hope to extend our current effort in microscopy to stand-off imaging to improve the frame rate of IR imaging for remote threat detection.

A QCL array was chosen as the light source for this system. QCL sources emit light at IR wavelengths, operate at room temperature, and produce milliwatts of radiation.[12] QCL sources are also lightweight and have low power requirements, making them ideal for systems that are being developed for security applications.[13] In this work we demonstrate that our hyperspectral microscope can use spectral information to distinguish between dichloromethane and water and that it is able to acquire a merged IR-visible image by combining the hyperspectral IR image with a high-resolution bright-field image generated with a visible laser source. We also present results of simulations and initial studies showing the benefit of using sparse-sampling in future work.[14]

Sparse sampling takes advantage of the high information redundancy in conventional images, such that much of the essential information content can be mapped into a much smaller sized basis set by image compression. Similarly, full images can often be reconstructed from a relatively small subsampling of pixels building on this inherent redundancy, with the results varying considerably depending on the quality of the reconstruction algorithm used and the signal to noise ratio of the sampled pixels. The advantages of Lissajous scanning are illustrated in **Fig. 1**, in which the trajectory used to sample pixels can have a profound impact in the subsequent ability to perform image reconstruction from sparse sampling. The bottlenecks for high-speed imaging can be reduced by orders of magnitude through maximizing the inherent information content per measurement acquired by sparse sampling, rather than maximizing the sheer volume of data obtained.

2. EXPERIMENTAL

2.1. Experimental instrumentation

The hyperspectral microscope is depicted in **Fig. 2**. In brief, a custom 32-channel LWIR QCL array with a wavenumber range of 1190–1340 cm^{-1} (Pendar Technologies) was used as the absorption light source. A 640 nm laser diode (Thorlabs)

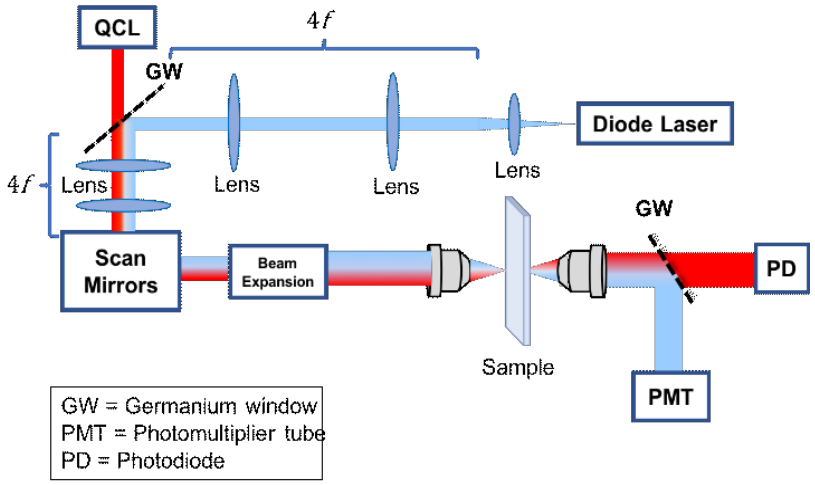

Figure 2. Instrument schematic of the LWIR hyperspectral microscope. 640 nm beam is emitted from the diode laser and is combined with 32-channel LWIR beam emitted from the QCL.

was used as the bright-field light source. The two laser beams were combined using a germanium window (Thorlabs). The 640 nm laser diode beam was 4f coupled to a germanium window with two lenses to enable fine adjustment of the collimation at the point of beam combination to correct for chromatic aberration. The copropagating beams were expanded twice with two sets of lenses and scanned across the sample using a pair of galvanometer mirrors (ScannerMAX). A 15 × 0.4 NA reflective Cassegrain objective (Edmund Optics) was used to focus the beams onto the sample. Light from the sample plane was recollimated using a collection lens and a germanium window was used to separate the 640 nm beam from the LWIR beam. 640 nm light was detected using a photomultiplier tube (Hamamatsu). LWIR light was detected using an LWIR-sensitive photodiode (Vigo System). IR compatible lenses (Thorlabs) were used when focusing the LWIR beam. Responses of the detectors were digitized synchronously with a 10 MHz clock using a digital oscilloscope card (AlazarTech). Custom software (MATLAB) was used to down-sample raw data to coincide with LWIR laser pulses and remap the down-sampled data onto a set of 256 pixel × 256 pixel LWIR images (one for each QCL channel) and one 256 pixel × 256 pixel 640 nm bright-field image. K-means clustering was used to assign chemical identity in images of mixtures. The high-resolution 640 nm image and the low-resolution LWIR images were combined using custom software (MATLAB) to create a merged image containing IR spectral information encoded in an RGB color map.

2.2. Sample preparation

Dichloromethane was purchased from Mallinckrodt. Dichloromethane was mixed with water and imaged on an IR-transparent calcium-fluoride slide. A 5 µm pig liver section was obtained from the Histology Research Laboratory at Purdue University and was imaged on an IR-transparent calcium-fluoride slide.

2.3. Sparse-sampling

Lissajous scan patterns for simulations were selected based on the available bandwidths of the corresponding scan mirrors. A 10223:11527 Lissajous trajectory was found to be an optimal sampling trajectory for image reconstruction. Experimental demonstration of sparse sampling was performed using an interleaved raster trajectory with 0.1% sampling of the field of view for each wavelength channel. In-painting of the unsampled pixels was performed using an in-painting algorithm based on the discrete cosine transform designed for applicability with data sets of arbitrary dimensionality developed by Garcia et al., with 1000 smoothness parameters between 6 and -6 used to reconstruct images using this algorithm.[15, 16]

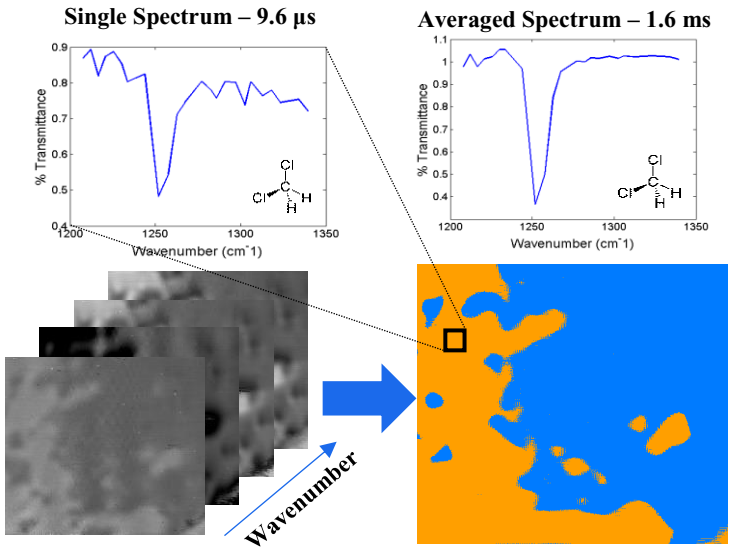

Figure 3. Spectroscopic imaging of water/dichloromethane mixture. A set of images are acquired representing 32 wavelengths of light. Chemical identity is assigned by at each pixel using k-means clustering.

3. RESULTS AND DISCUSSION

3.1. LWIR hyperspectral imaging

A water/dichloromethane mixture was used to assess the hyperspectral imaging of the system and the accuracy of the classification algorithm. Images were acquired using conventional raster scanning without sparse sampling. **Fig. 3** shows some of the IR images that were acquired, representing 32 wavelengths of LWIR light. The images are correlated so that each pixel contains a spectrum. Each pixel was assigned a chemical identity based on its spectral information using k-means clustering. The strong absorption band of dichloromethane at 1250 cm^{-1} easily distinguishes it from water in the spectral domain. The classified image matches qualitatively with the LWIR images and the spectra shown match the literature IR spectrum for dichloromethane.[17] The LWIR imaging system can acquire a spectrum in 9.6 μs and a signal-averaged spectrum (using 50 spectra) in 1.6 ms. This corresponds to a total image acquisition time of approximately two

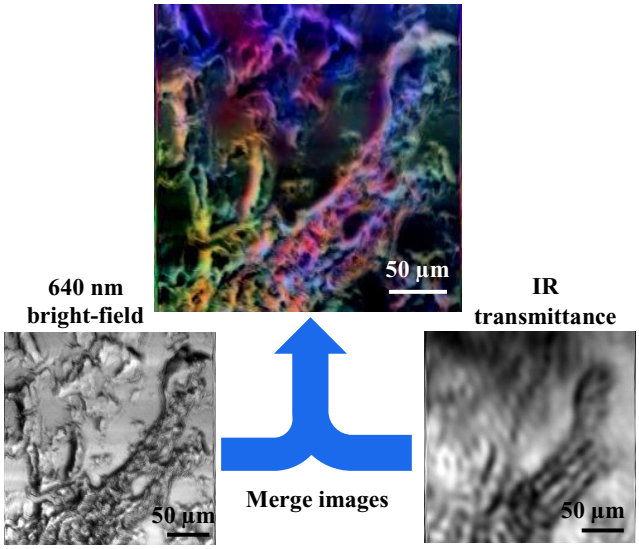

Figure 4. Merged IR-visible imaging. 640 nm bright-field image contained high-resolution features and LWIR images contain spectral information. Merged image retains information from both images.

seconds using conventional raster scanning for a 256 pixel × 256 pixel × 32 channel hyperspectral image stack. These results demonstrate that the LWIR imaging system can rapidly acquire hyperspectral images and use spectral information to distinguish between chemical entities.

3.2. Merged IR-visible imaging

A 5 μm pig liver section was analyzed to assess the imaging capabilities of the hyperspectral microscope when using both the LWIR beam and the 640 nm visible beam. Conventional raster scanning was used during the acquisition of these images. **Fig. 4** shows that data from both light sources were used to produce the merged images. The 640 nm bright field image contains high-resolution features and the LWIR transmittance image contains spectral information, but with low spatial resolution. These two images were merged using custom software to produce an image with the high-spatial resolution of the 640 nm image encoded with spectral information from the LWIR images in an RGB color map. This image demonstrates the ability of this microscope to simultaneously capture high-resolution detail and spectral content in the LWIR.

3.3. Sparse-sampling simulations

To evaluate the advantage of sparse sampling with the LWIR hyperspectral microscope, image reconstructions with known ground-truth results were performed for three different beam-scanning trajectories: random-access sampling, Lissajous scanning, and interleaved raster scanning. For the random-access sampling, random pixels within the field of view were chosen to be sampled. For Lissajous scanning, sinusoidal functions with optimized phases and periods on both axes were

used to map the trajectory of the beam across the field of view. For the interleaved raster scanning, the trajectories were assumed to be bidirectional (i.e., the trace and retrace recorded on separate lines) with no dead time associated with the slow-axis repositioning between lines. Quantitative analysis of the errors arising in the reconstructions as a function of the

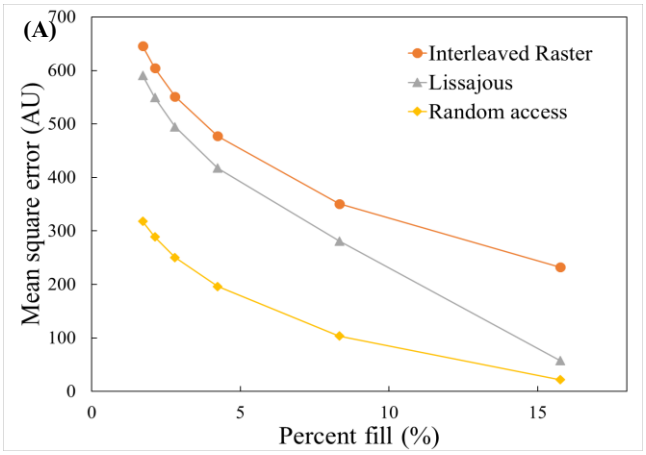

Figure 5. Simulation of the reconstruction error associated with various sparse sampling methods. (A) Plot of reconstruction error versus sampling percentage. (B) Still frames selected from in-painting based on a discrete cosine transformation for different assumed sampling trajectories.

percentage of sampling is shown in **Fig. 5A**. Consistent with the qualitative expectations from inspection of the images in **Fig. 5B**, the random-access trajectory provides the least reconstruction errors, followed by Lissajous, and then interleaved raster. The performances of the different trajectories illustrated in **Fig. 5** are generally weighed against the practical constraints associated with beam-scanning hardware. For example, the potential advantages of random-access sampling are tempered by the difficulties in practically achieving full random-access sampling with negligible dead-time for beam repositioning. Continuous line-scanning trajectories represented by the Lissajous and approximated by the interleaved sampling strategies are considerably simpler to achieve in practice using simple and common mirror assemblies.

3.4. Sparse-sampling measurements

Initial measurements utilizing sparse-sampling trajectories were acquired with the LWIR hyperspectral microscope. **Fig. 6** shows sparsely-sampled and reconstructed images of a 1951 USAF resolution test target. An interleaved raster trajectory was used with 0.1% sampling of the field of view for each wavelength channel. The sparse image is so under-sampled that it is difficult to detect by eye any signal. A zoom-in of the sparse image reveals pixels that have been sampled. In-painting of the sparse image was performed using an algorithm based on the discrete cosine transform to produce the reconstructed image. The reconstructed image qualitatively resembles the test target, blurred due to the diffraction limit. This interpolated image demonstrates that frame rate can be significantly increased by reducing sampling without significant reduction in image quality.

4. CONCLUSIONS

A LWIR hyperspectral microscope was developed with 32 spectral channels with a wavenumber range of 1190–1340 cm^{-1} and a total image acquisition time of approximately two seconds using conventional raster scanning for a 256 pixel × 256 pixel × 32 channel hyperspectral image stack. K-means clustering enabled classification of spectra and assignment of chemical identity with no prior knowledge of the sample. Good agreement was observed between the recovered spectra and those in the literature. Merging LWIR images with 640 nm bright field images enhanced the resolution of features in the images while retaining spectral information. Simulations of sparse-sampling methods suggest that Lissajous scanning can improve frame rate and result in less reconstruction error than interleaved raster scanning. Initial measurements demonstrate that sparse sampling can reduce image acquisition time without significant reduction in

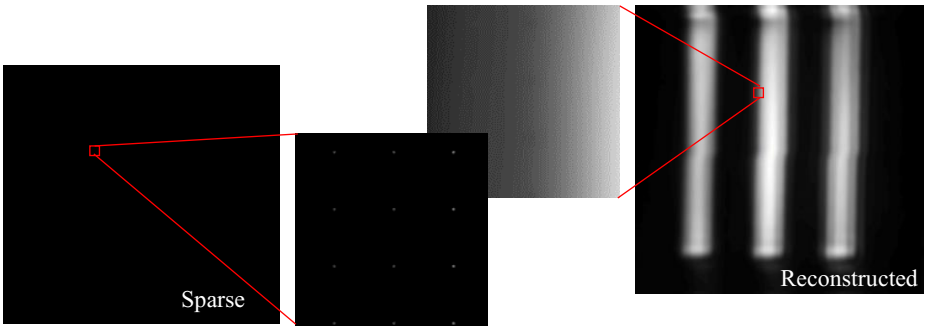

Figure 6. Sparse sampling and in-painting of 1951 USAF resolution test target. A sparse raster trajectory was used to sample the test target. Sparse image shows signal at a low percentage of discrete pixels in the field of view. Reconstructed image demonstrates that frame rate can be significantly increased by reducing sampling without significant reduction in image quality.

image quality by using in-painting. Future work will involve improving algorithms for merging visible and LWIR images and implementing Lissajous scanning into the LWIR hyperspectral microscope for leveraging all four accessible dimensions (x, y, time, wavelength) during image reconstruction to further improve frame rate.

ACKNOWLEDGMENTS

The authors graciously acknowledge support from NSF GOALI 109173, Purdue Research Foundation, and Pendar Technologies LLC.

REFERENCES

[1] Colton, R. J.; Russell, J. N., Making the world a safer place. Science 2003, 299 (5611), 1324-1325.
[2] Hallowell, S. F., Screening people for illicit substances: a survey of current portal technology. Talanta 2001, 54 (3), 447-458.
[3] Yinon, J., Counterterrorist detection techniques of explosives. Elsevier: 2011.
[4] Bauer, C.; Sharma, A. K.; Willer, U.; Burgmeier, J.; Braunschweig, B.; Schade, W.; Blaser, S.; Hvozdara, L.; Muller, A.; Holl, G., Potentials and limits of mid-infrared laser spectroscopy for the detection of explosives. Applied Physics B-Lasers and Optics 2008, 92 (3), 327-333.
[5] Moon, D. E.; Tazik, S. K.; Wierszewski, J. G.; Gomer, N. R.; Nelson, M. P. In Novel use of shortwave infrared hyperspectral imaging for standoff detection of explosives and narcotics in room clearing applications, Next-Generation Spectroscopic Technologies XI, International Society for Optics and Photonics: 2018; p 106570T.
[6] Breshike, C. J.; Kendziora, C. A.; Furstenberg, R.; Nguyen, V.; Kusterbeck, A.; McGill, R. A. In Using infrared backscatter imaging spectroscopy to detect trace explosives at standoff distances, Chemical, Biological,

Radiological, Nuclear, and Explosives (CBRNE) Sensing XIX, International Society for Optics and Photonics: 2018; p 106290N.
[7] Wood, D.; Kelley, D.; Goyal, A.; Kotidis, P. In Mid-infrared reflection signatures for trace chemicals on surfaces, Chemical, Biological, Radiological, Nuclear, and Explosives (CBRNE) Sensing XIX, International Society for Optics and Photonics: 2018; p 1062915.
[8] Ewing, K. J.; Major, K. J.; Sanghera, J. S.; Gattass, R. R.; Shaw, L. B.; Busse, L.; Arnone, D.; Lopez, E.; Pushkarsky, M.; Kane, J. In Enabling standoff detection of hazardous materials using a fiber optic coupled quantum cascade infrared laser system, Chemical, Biological, Radiological, Nuclear, and Explosives (CBRNE) Sensing XIX, International Society for Optics and Photonics: 2018; p 106290A.
[9] Armougom, J.; Melkonian, J.-M.; Dherbecourt, J.-B.; Raybaut, M.; Grisard, A.; Lallier, E.; Gérard, B.; Faure, B.; Souhaité, G.; Boulanger, B. J. A. P. B., A narrowband infrared source based on orientation-patterned GaAs for standoff detection of chemicals. 2018, 124 (7), 133.
[10] Nelson, M. P.; Tazik, S. K.; Treado, P. J.; Zhi, T.; Narasimhan, S.; Pires, B.; Hebert, M. In Real-time, short-wave, infrared hyperspectral conforming imaging sensor for the detection of threat materials, Next-Generation Spectroscopic Technologies XI, International Society for Optics and Photonics: 2018; p 106570U.
[11] Breshike, C. J.; Kendziora, C. A.; Furstenberg, R.; Nguyen, V.; Kusterbeck, A.; McGill, R. A. In A system for rapid chemical identification based on infrared signatures, Micro-and Nanotechnology Sensors, Systems, and Applications X, International Society for Optics and Photonics: 2018; p 1063927.
[12] Goyal, A. K.; Kotidis, P.; Deutsch, E. R.; Zhu, N.; Norman, M.; Ye, J.; Zafiriou, K.; Mazurenko, A. In Detection of chemical clouds using widely tunable quantum cascade lasers, Chemical, Biological, Radiological, Nuclear, and Explosives (CBRNE) Sensing XVI, International Society for Optics and Photonics: 2015; p 94550L.
[13] Witinski, M. F.; Blanchard, R.; Pfluegl, C.; Diehl, L.; Li, B.; Krishnamurthy, K.; Pein, B. C.; Azimi, M.; Chen, P. L.; Ulu, G.; Rhodes, G. V.; Howle, C. R.; Lee, L.; Clewes, R. J.; Williams, B.; Vakhshoori, D., Portable standoff spectrometer for hazard identification using integrated quantum cascade laser arrays from 6.5 to 11 mu m. Optics Express 2018, 26 (9), 12159-12168.
[14] Geiger, A. C.; Newman, J. A.; Sreehari, S.; Sullivan, S. Z.; Bouman, C. A.; Simpson, G. J. In Sparse sampling image reconstruction in Lissajous trajectory beam-scanning multiphoton microscopy, Conference on High-Speed Biomedical Imaging and Spectroscopy - Toward Big Data Instrumentation and Management II, San Francisco, CA, Jan 30-Feb 01; San Francisco, CA, 2017.
[15] Garcia, D., Robust smoothing of gridded data in one and higher dimensions with missing values. Computational Statistics & Data Analysis 2010, 54 (4), 1167-1178.
[16] Wang, G. J.; Garcia, D.; Liu, Y.; de Jeu, R.; Dolman, A. J., A three-dimensional gap filling method for large geophysical datasets: Application to global satellite soil moisture observations. Environmental Modelling & Software 2012, 30, 139-142.
[17] Spectral Database for Organic Compounds (SDBS); infrared spectrum; SDBS No.: 891; RN 75-09-2; https://sdbs.db.aist.go.jp/sdbs/cgi-bin/landingpage?sdbsno=891 (accessed August 6, 2018).